Picosecond anti-Stokes generation in a photonic-crystal fiber for interferometric CARS microscopy

Esben Ravn Andresen

Department of Physics and Astronomy, University of Aarhus, Ny Munkegade, DK-8000 Aarhus C, Denmark

Søren Rud Keiding

Department of Chemistry, University of Aarhus, Langelandsgade 140, DK-8000 Aarhus C, Denmark

Eric Olaf Potma

Department of Chemistry & Beckman Laser Institute, University of California Irvine, Irvine, CA 92697, USA

Abstract: We generate tunable picosecond anti-Stokes pulses by four-wave mixing of two picosecond pump and Stokes pulse trains in a photonic-crystal fiber. The visible, spectrally narrow anti-Stokes pulses with shifts over 150 nm are generated without generating other spectral features. As a demonstration, we employ the generated anti-Stokes pulses as reference pulses in an interferometric coherent anti-Stokes Raman scattering imaging experiment showing that interpulse coherence among the pump, Stokes and anti-Stokes beams is retained.

OCIS codes: (060.4370) Nonlinear optics, fibers, (180.3170) Interference microscopy, (300.6230) Spectroscopy, coherent anti-Stokes Raman scattering

---

References and links

1. A.V. Husakou and J. Herrmann, "Supercontinuum generation, four-wave mixing, and fission of higher-order solitons in photonic-crystal fibers", J. Opt. Soc. Am. B, **19**, 9, 2171-2182 (2002).
2. G.P. Agrawal, *Nonlinear fiber optics*, (Academic Press Limited, London, 1995).
3. M.E. Marhic, N. Kagi, T.-K. Chiang, and L.G. Kazovsky, "Broadband fiber optical parametric amplifiers", Opt. Lett., **21**, 8, 573-575 (1996).
4. S. Wabnitz, "Broadband Parametric Amplification in Photonic Crystal Fibers With Two Zero-Dispersion Wavelengths", J. Lightwave Tech., **24**, 4, 1732-1738 (2006).
5. T.V. Andersen, K.M. Hilligsøe, C.K. Nielsen, J. Thøgersen, K.P. Hansen, S.R. Keiding, and J.J. Larsen, "Continous-wave wavelength conversion in a photonic crystal fiber with two zero-dispersion wavelengths", Opt. Exp., **12**, 17, 4113-4122 (2004).
6. J.E. Sharping, M.Fiorentino, A. Coker, and P. Kumar, "Four-wave mixing in microstructure fiber", Opt. Lett., **26**, 1048-1050 (2001).
7. C.H. Kwok, S.H. Lee, K.K. Chow, C. Shu, C. Lin and A. Bjarklev, "Widely tunable wavelength conversion with extinction ratio enhancement using PCF-based NOLM", IEEE Photon. Techn. Lett. **17**, 2655-2657 (2005).
8. A. Zhang and M.A. Demokan, "Broadband wavelength converter based on four-wave mixing in a highly nonlinear photonic crystal fiber", Opt. Lett. **30**, 2375-2378 (2005).
9. G.L. Eesley, M.D. Levenson, and W.M. Tolles, "Optically Heterodyned Coherent Raman Spectroscopy", IEEE J. Q. El., **14**, 1, 45-49 (1978).
10. E.O. Potma, C.L. Evans, and X. Sunney Xie, Opt. Lett., "Heterodyne coherent anti-Stokes Raman scattering (CARS) imaging", **31**, 2, 241-243 (2006).
11. D.L. Marks, C. Vinegoni, J.S. Bredfeldt, and S.A. Boppart, "Interferometric differentiation between resonant coherent anti-Stokes Raman scattering and nonresonant four-wave-mixing processes", Appl. Phys. Lett., **85**, 23, 5787-5789 (2004).

12. C.L. Evans, E.O. Potma, and X.S. Xie, "Coherent anti-Stokes Raman scattering (CARS) spectral interferometry: Determination of the real and imaginary components of the nonlinear susceptibility for vibrational microscopy", Opt. Lett. **29** , 2923-2925 (2004).

13. S.H. Lim, A. Caster, S.R. Leone, "Single pulse phase-control interferometric coherent anti-stokes raman scattering spectroscopy (CARS)", Phys. Rev. A, **72**, 041803(1-4) (2005)

14. T.W. Kee, H. Zhao, and M.T. Cicerone, "One-laser inferferometric broadband coherent anti-Stokes Raman scattering", Opt. Express, **14**, 3631-3636 (2006).

15. V.V. Krishnamachari, E.R. Andresen, S.R. Keiding, and E.O. Potma, "An active interferometer-stabilization scheme with linear phase control", Opt. Exp. **14**, 5210-5215 (2006).

16. S. Diddams and J.C. "Dispersion measurements with white-light interferometry", J. Opt. Soc. Am. B, **13**, 6, 1120-1129 (1996).

17. J.M. Dudley, S. Coen, "Coherence properties of supercontinuum spectra generated in photonic crystal and tapered optical fibers", Opt. Lett., **27**, 13, 1180-1182 (2002).

18. J.W. Hahn and E.S. Lee, "Measurement of nonresonant third-order susceptibilities of various gases by the nonlinear interferometric technique", J. Opt. Soc. Am. B, **12**, 6, 1021-1027 (1995).

1. Introduction

Photonic crystal fibers (PCF)s have attracted a lot of attention because of their enhanced non-linearity and novel dispersion properties compared to standard fibers. In particular the generation of supercontinua in PCFs has been widely studied [1]. Less emphasis has been put on narrow-band frequency conversion of picosecond pulses. The development of efficient conversion schemes for the generation of spectrally tunable, picosecond pulses would be of considerable interest to various fields of research, including picosecond coherent Raman spectroscopy.

Anti-Stokes generation in optical fibers is a promising mechanism for frequency conversion of ps-pulses. A four-wave mixing (FWM) technique, anti-Stokes generation involves a pump and a Stokes wave at frequencies ω_p and ω_S, respectively, to produce a signal wave at $2\omega_p - \omega_S$. In standard fibers, anti-Stokes generation has been used to parametrically shift the frequency around the telecommunication wavelength.[2, 3] FWM in PCFs [6] can exhibit much larger anti-Stokes shifts than in standard fibers [1, 4, 5]. Using PCFs, anti-Stokes shifts over several tens of nanometers was demonstrated around 1550 nm [4, 7, 8] and several hundred nm around 800 nm. [5].

This earlier work has mainly focused on cw radiation or on pulses that are too long to be of interest to many types of nonlinear spectroscopy. In this work we show that anti-Stokes shifts of several hundred nm can be obtained in a short PCFs for ~ 10 ps pulses. It is emphasized that the anti-Stokes generation takes place without competing nonlinear effects or temporal broadening. We demonstrate that the coherence between the generated anti-Stokes pulse and the pump and Stokes pulses is retained after the fiber by applying it to interferometric coherent anti-Stokes Raman scattering (CARS) microscopy.

CARS interferometry is based on mixing the CARS field with a controllable anti-Stokes local oscillator field [9]. This allows for elimination of the nonresonant background in CARS microscopy and for exclusive detection of the vibrationally resonant contribution to the signal, both in narrowband [10] and broadband configurations.[11, 12, 13, 14] In previous picosecond interferometric CARS studies, the local oscillator was generated with low efficiency in a non-resonant liquid sample.[10] In addition, phase drift in the interferometer may compromise the accuracy of the technique unless an active stabilization scheme is being used [15]. We show that a simple and stable CARS interferometer can be constructed by employing the efficiently generated anti-Stokes radiation in the PCF as the local oscillator.

2. Picosecond anti-Stokes generation

We use a 16 mm-long piece of single-mode polarization-maintaining PCF (Crystal Fibre A/S, Denmark) with zero-dispersion wavelengths (ZDW)s at 780 nm and 1100 nm. This fiber has a
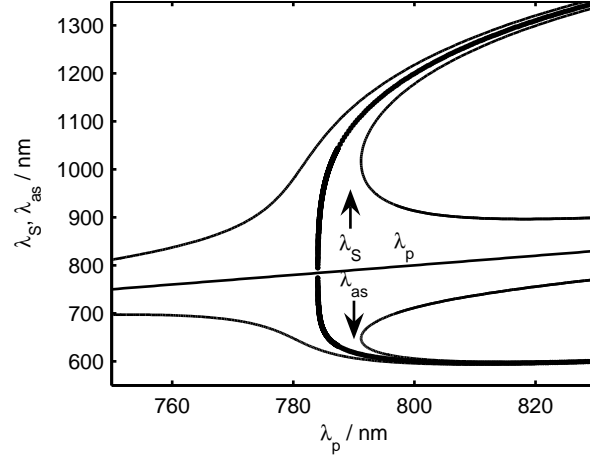
Fig. 1. Phase-matching for FWM in the PCF. The thick line corresponds to $\Delta\beta = 0$, the thin line to $|\Delta\beta L/2| = \pi/2$.

nonlinear coefficient $\gamma = 0.095\,(\mathrm{Wm})^{-1}$ and the core diameter is 1.7 μm.

We study the case where picosecond pump and Stokes pulses are co-propagating in the PCF. Generation of signal the anti-Stokes frequency, $\omega_{as} = 2\omega_p - \omega_S$, is governed by the wave-vector mismatch,

$$\Delta\beta = \beta_{as} + \beta_S - 2\beta_p. \tag{1}$$

for efficiency to be high, $\Delta\beta$ must be small. The group-velocity dispersion of the fiber, β_2 versus wavelength was measured by white-light interferometry. [16] By integration of β_2, we obtain the wavelength dependence of β. From $\beta(\lambda)$, we find the combinations of pump, Stokes, and anti-Stokes wavelengths that fulfill the phase-matching criterion for FWM, $\Delta\beta = 0$. The phase-matching curve for FWM in this fiber is shown in Fig. 1.

In the limiting case of no pump depletion and at low pump power, the reference signal power can be written as [2]

$$P_{as} = G_a P_S, \tag{2}$$

where G_a is the single-pass gain,

$$G_a = P_{as}(L)/P_S(0) = (\gamma P_p)^2 \frac{\sin^2(\Delta\beta L/2)}{(\Delta\beta/2)^2}. \tag{3}$$

P_p and P_S are the pump and Stokes powers and L the fiber length. The present short fiber length leads to a broad range of $\Delta\beta$ or, equivalently, pump wavelengths, for which FWM takes place with significant efficiency. Using 40 mW radiation at 816.3 nm and 60 mW Stokes power at 1064 nm in the fiber, we generate 1 μW of anti-Stokes signal at 662 nm. This is 3 orders of magnitude greater than what has been reported using a nonresonant CARS sample. Similar efficiencies are obtained over a range for tuning the pump pulse 40 nm close to the ZDW, which corresponds to a 600 cm^{-1} range of vibrational frequency. G_a has significant magnitude, even when λ_p is so that $|\Delta\beta L/2| > \pi/2$. The results are summarized in Fig. 2. The inset signifies that the anti-Stokes pulse is generated exclusively, without generation of other spectral features.

The short PCF and its dispersion properties imply that chirp and nonlinear effects besides FWM can be neglected. Spectral broadening of the pulses is expected to occur for a nonlinear interaction length $L_{nl} = 1/(\gamma P)$ of $\sim$100 mm. The dispersion length, $L_D = \tau_0^2/|\beta_2| \sim 10^4$ for all pulses, shows that chirp effects are negligible. The group delay walkoff, $L(\beta_1(\lambda_1) - \beta_1(\lambda_2))$,
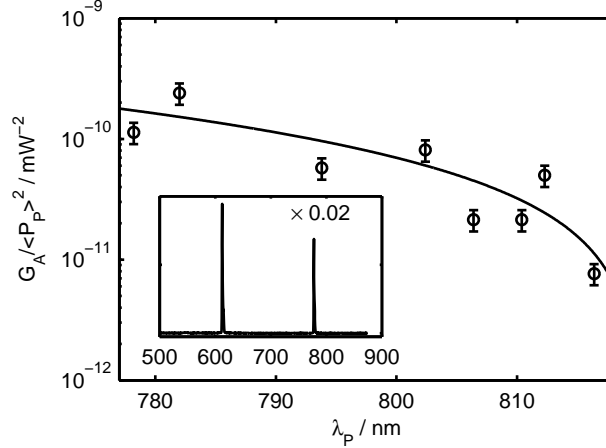
Fig. 2. Single-pass gain in the PCF normalized to average pump power squared. The solid line is a guide for the eye. The inset shows a representative pump (778 nm) and anti-Stokes (613 nm) spectrum after the PCF. The Stokes at 1064 nm is not shown.

between the pump and Stokes pulses is ~ 1000 fs, while between the pump and reference pulses, it is ~ 200 fs. Compared to the pulse durations of ~ 7 ps, this is negligible.

We note that the generation of a well-defined spectral feature in a PCF without generation of additional features is atypical for pulses of duration of a few picoseconds. PCFs have attracted interest mainly as a means of generating supercontinua [1]. PCF-generated supercontinua are known to be noisy under certain conditions [17], when picosecond pumping is used. That particular noise is of no concern here, as it does not arise from FWM.

3. Interferometric coherent anti-Stokes Raman scattering

The experimental setup is shown in Fig. 3. The Stokes beam is derived from a 76 MHz, 7-ps modelocked Nd:Vandate laser at 1064 nm. A ps-synchronously pumped optical parametric oscillator provides the tunable pump beam (775 - 820 nm) for the CARS process. Both the pump and Stokes are coupled into the PCF with a microscope objective. After the PCF, the pump, Stokes and anti-Stokes reference are collinearly coupled into a laser scanning microscope. The CARS signal at the detector is given as:

$$S \quad \propto \quad 2(\mathrm{Re}\chi_r^{(3)} + \chi_{nr}^{(3)})E_{ref}E_p^2E_S\cos(\Phi) + 2\mathrm{Im}\chi_r^{(3)}E_{ref}E_p^2E_S\sin(\Phi)$$
$$[+\mathrm{non-interferometric\ terms}],$$

where $\chi_r^{(3)}$ and $\chi_{nr}^{(3)}$ are the resonant and nonresonant contributions to the nonlinear susceptibility, respectively, and Φ is the relative phase between the anti-Stokes and reference field. A wedge plate provides a means for tuning Φ. Although not used here, the interferometric terms can, in principle, be separated from the non-interferometric terms by using phase-modulation of one of the fields combined with lock-in detection. [10] Setting $\Phi = \pi/2$ allows exclusive detection of the imaginary part of $\chi^{(3)}$, while $\Phi = 0$ selects the real contribution of $\chi^{(3)}$. $\mathrm{Im}\chi_r^{(3)}$ yields the Raman spectrum, linear in concentration of the species under study and free of non-resonant background. [9] The wedge prisms introduce an additional delay of 170 to 670 fs between the pump and Stokes, and 120 to 480 fs between the reference and the pump. This is negligible compared to the pulse durations. Changing the wedge position to change Φ by $\pi/2$ changes interpulse delays only by few fs. A similar setup has been reported previously [18],
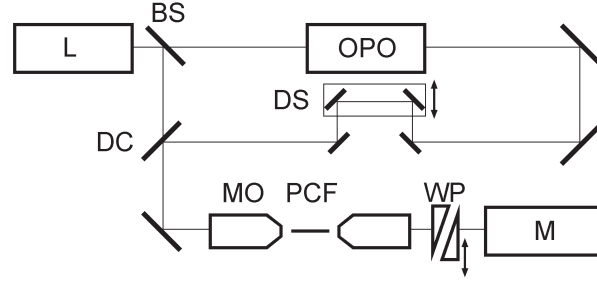
Fig. 3. Experimental setup. L: Laser (PicoTrain, High-Q Lasers); OPO: Optical parametric oscillator (Levante, APE Berlin); BS: Beam splitter; DS: Delay stage; DC: Dichroic mirror; MO: Microscope objective (0.66 NA, Leica Achro 40×); PCF: Photonic-crystal fiber; WP: Wedge prism pair (10°, BK7); M: Microscope (FluoView 300, Olympus).
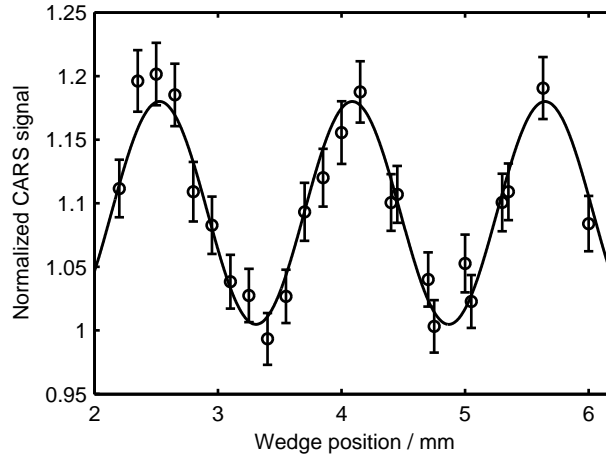

Fig. 4. Average signal inside a dodecane droplet normalized to average signal in the surrounding water versus wedge position. The solid line is a sinusoidal fit to the points.

in that report, a 10 Hz nanosecond laser system was used, making their setup better suited for CARS spectroscopy of gases than microscopy.

To demonstrate that interpulse coherence is retained as well as the utility of the PCF-generated anti-Stokes reference field for CARS microscopy, we record interferometric images of dodecane droplets in water. Setting the pump wavelength to 816.3 nm and the Stokes to 1064 nm, a Raman shift of 2852 cm^{-1} is selected, coinciding with the CH_2 vibration frequency of dodecane. The CARS signal from the dodecane droplets is predominantly resonant signal, while the surrounding water produces only nonresonant signal. The signal intensity from the dodecane droplet is

$$S \propto |\chi_r^{(3)}|^2 I_p^2 I_S + |E_{ref}|^2 + 2\varepsilon \mathrm{Im}\chi^{(3)} E_p^2 E_S E_{ref} \sin\Phi \qquad (4)$$

where ε is a constant that accounts for imperfect interference between the reference and anti-Stokes fields. It has been assumed that the reference and resonant signals are much stronger than the nonresonant signals so that terms containing $\chi_{nr}^{(3)}$ can be neglected. Fig. 4 shows the average interferometric signal from dodecane as a function of the wedge position. The points oscillate around a value slightly higher than 1. This agrees with Eq. 4, from which it is expected that
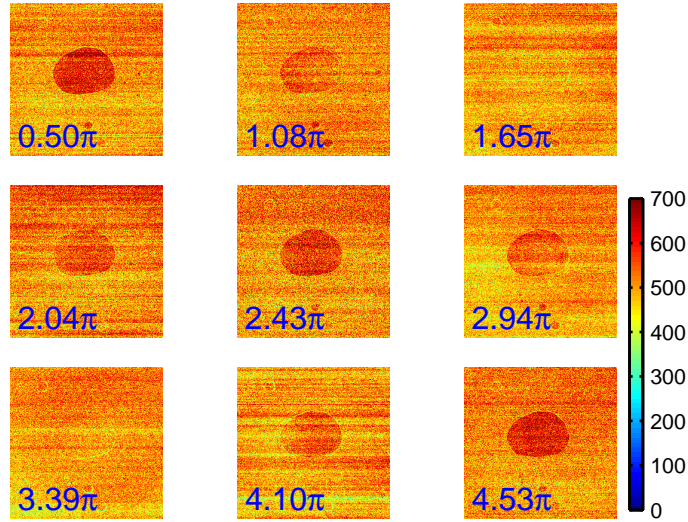
Fig. 5. Interferometric CARS images of a dodecane droplet in water. The labels denote Φ. Each image is 256×256 pixels or 175×175 μm. Acquisition time was 2.6 s/image. Pump and Stokes powers at the sample were 2.0 and 4.1 mW, respectively.

the points oscillate around $1 + |\chi_r^{(3)}|^2 I_p^2 I_S^2 / |E_{ref}|^2$. This result underlines that phase coherence between the incident pulses and the anti-Stokes reference generated in the PCF is retained.

Images for various settings of Φ are shown in Fig. 5. The series of images shows the recurring maxima and minima of the intensity of the central dodecane droplet. The images are reproducible for each position of the wedge, indicating that no phase drift occurs. There is some noise in the images, due to the low power in the sample plane, which again was due to a poorly reflecting element in the microscope.

4. Conclusion

In conclusion, we demonstrated that spectrally well-defined wavelength-tunable picosecond pulses at the anti-Stokes wavelength can be efficiently and exclusively generated in a PCF from pump and Stokes pulses. A significantly wider tuning range could be obtained, if a laser system were employed, where the pump wavelength could be held fixed near the ZDW, while the Stokes wavelength were tuned, as is apparent from Fig. 2. Phase coherence is retained, which permits a simple form of interferometric CARS microscopy, absent of any phase drift. If required, our simplified scheme can be improved by implementing phase modulation and lock-in detection through mounting one of the wedge prisms on a shaker. Our anti-Stokes generation scheme can also be easily incorporated in a Mach-Zender-type setup for CARS interferometry[10], constituting an efficient alternative to the previously used liquid samples for anti-Stokes generation.